Published in final edited form as:
Org Lett. 2020 August 07; 22(15): 6150–6154. doi:10.1021/acs.orglett.0c02213.

Photophysical tuning of shortwave infrared flavylium heptamethine dyes via substituent placement

Monica Pengshung[1], **Jingbai Li**[2], **Fatemah Mukadum**[2], **Steven A. Lopez**[2,*], **Ellen M. Sletten**[1,*]

[1]Department of Chemistry and Biochemistry, University of California, Los Angeles, 607 Charles E. Young Drive East, Los Angeles, California 90095, United States.

[2]Department of Chemistry and Chemical Biology, Northeastern University, 360 Huntington Avenue, Boston, Massachusetts 02115, United States.

Abstract

Optical imaging in the shortwave infrared (SWIR, 1000–2000 nm) region of the electromagnetic spectrum provides high resolution imaging in complex systems. Here, we explore substituent placement on dimethylamino flavylium polymethine dyes, a class of SWIR fluorophores. We find that the position of substituent affects the λ_{max} and fluorescence quantum yield. Quantum mechanical calculations suggest that steric clashes control the extent of π-conjugation. These insights provide a design principle for the development of novel fluorophores for enhanced SWIR imaging.

Graphical Abstract

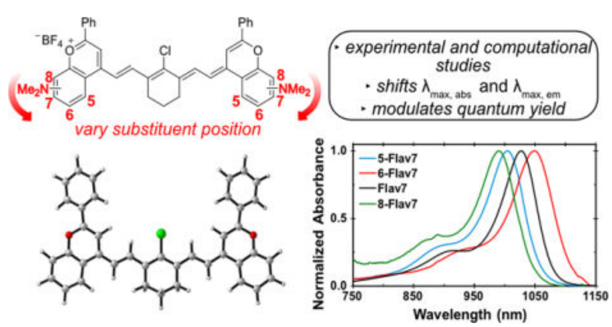

*Corresponding Author: s.lopez@northeastern.edu. sletten@chem.ucla.edu.

Author Contributions

M.P. and E.M.S. designed the study. M.P. performed synthesis and measured photophysical properties. J.L and F. M. performed the quantum mechanical calculations and J.L. completed the analysis of the substituent effects on the photophysical proper-ties. M.P., J. L, S. L. and E.M.S wrote and edited the paper. All authors have given approval to the final version of the manu-script.

Supporting Information

Experimental procedures, supplemental Figures S1–3, full spec-troscopic data and computational analysis for compounds are included in the supporting information.

Introduction

Fluorophores in the shortwave infrared (SWIR, 1000–2000 nm) region of the electromagnetic spectrum have recently garnered excitement as tools for biological imaging.[1–3] The SWIR region is advantageous for optical imaging in complex systems because of the increased depth penetration of light through tissue, enhanced image resolution, and low energy photons as compared with the visible and near-infrared regions.[4,5] Imaging in the SWIR originally necessitated single-wall carbon nanotubes (SWCNT)[6–9], rare earth nanomaterials[10–12] and quantum dots[13–15] as contrast agents, which have biocompatibility or bioaccumulation concerns.[11, 16–19] In contrast with these nanostructures, small molecule fluorophores have low toxicity and are readily cleared from the body.[20] However, it is challenging to obtain fluorophores with absorption and emission above 1000 nm with fluorescence quantum yields (Φ_F) greater than ~0.3%.[21–23]

In 2017, we reported a bright flavylium heptamethine SWIR fluorophore, deemed **Flav7** (**1**, Figure 1).[24] **Flav7** contains a dimethylamino substituent at the seven-position, which provided a λ_{max} above 1000 nm. Recently, we have varied the electron-donating substituent at the seven-position and found that the $\lambda_{max,abs}$ can be modulated by ~80 nm and form a linear free energy relationship with σ *meta* Hammett constants.[25] The identity of the substituent had minimal effect on the quantum yield of the series analyzed (Φ_F = 0.42–0.62%). Finding that the seven-position represented the *meta*-position prompted our interest in placing the dimethylamino group at other positions on the flavylium heterocycle (Figure 1). Additional π-donation resulting from *para* and *ortho* substitution can lead to more significant electronic contributions from substituents, although the *ortho* position can be complicated by sterics.[26] Herein, we report how dimethylamino substituents at putative *ortho*-, *meta*-, and *para*-positions on flavylium heptamethine fluorophores affect photophysical properties exploring experimental and quantum mechanical analyses.

Results and Discussion

The dimethylamino flavylium heptamethine dyes were synthesized by leveraging chemistry developed to access **Flav7** derivatives.[25] The dimethylamino group was installed through a Buchwald Hartwig amination from either triflated or brominated flavones (**6a-c**) to provide dimethylamino substituents at the five-, six-, or eight-position (**7a-c**), respectively (Scheme 1). The addition of methyl-Grignard followed by quenching with tetrafluoroboric acid yielded flavylium hetereocycles (**8a-c**), which could then be treated with linker **9** and 2,4-di-*tert*-butyl-4-methylpyridine to provide **5-, 6-**, and **8-Flav7** (**3–5**, respectively). These dyes are named with the first number representing the position of the dimethylamino substituent on the flavylium heterocycle, and Flav7 references the flavylium heptamethine.

We isolated pure **5-Flav7** (**3**) and **6-Flav7** (**4**). However, the eight-substituted flavylium (**8c**) readily reacted with oxygen to form a monomethine dye, characterized by an absorption peak at 722 nm (Figure S1).[24] To minimize this, crude **8c** was immediately taken to the next reaction. The resulting **8-Flav7 (5)** proved difficult to purify due to its instability.[27] Thus, we gained as much photophysical information as possible from the crude sample. The absorption coefficient (ε) was not determined due to insufficient purity.

We evaluated the photophysical properties of the newly synthesized dyes in comparison with **Flav7** (**1**, Figure 2). The absorbance and emission spectra clearly show that the position of the dimethylamino affect the $\lambda_{max,abs}$ and $\lambda_{max,em}$. Previously, we correlated the seven-position with the *meta* position through Hammett analysis.[25] We expected that the six-position would correspond to the *para*-position and that substituent at this position would show pronounced effects due to enhanced π-donation. Indeed, we observed this result, as **6-Flav7** (4, Figure 2, red) is 20 nm bathochromically shifted from **Flav7** (**1**, Figure 2, black).

We then reasoned that the five-position could serve as the other *meta* position and the eight-position would be the *ortho* position. We expected that the absorption and emission of **5-Flav7** (**3**) would be similar to **Flav7** (**1**), and the same comparison could be drawn for **8-Flav7** (**5**) and **6-Flav7** (**4**). However, we observed that both **3** and **5** were hypsochromically shifted in comparison to **Flav7** (**1**). **5-Flav7** (3, Figure 2, blue) has a $\lambda_{max,abs}$ of 1004 nm, a blue shift of 23 nm from **Flav7** (**1**). **8-Flav7** (**5**, Figure 2, green) has a $\lambda_{max,abs}$ at 990 nm, nearly identical to parent dye **IR-27** (**2**). These results were counterintuitive to predicted $\lambda_{max,abs}$ based on Hammett parameters and prompted a quantum mechanical study.

We performed a conformational search of 10,000 structures enforcing the all-*trans* configuration along the polymethine chain while searching conformational flexibility of the phenyl groups (Refer to SI). We optimized the ten lowest conformers of each molecule with the M06–2X[28] density functional and the 6–31+G(d,p) basis set. We used the integral equation formalism polarizable continuum model (IEFPCM)[29] for all calculations in the presence of dichloromethane. The computed range of free energies between the ten lowest energy conformers is 0.0–0.7 kcal mol^{-1} (Figure S2).

To evaluate the photophysical properties, we used the global minima for **Flav7** dyes (**1**, **3–5**) as well as unmodified **IR-27** (**2**). The conjugated C-C bonds in the polymethine chains ranged from 1.39–1.41 Å. However, the substituents altered the planarity of the π-system along the polymethine chain and the flavylium heterocycle. We deconvoluted these effects with two angular parameters, α and β (Figure 3A,B). We define α as the angle between the plane of the polymethine and the plane of the flavylium, whereas β is the angle between the plane of the flavylium and the substituent. Analysis of the α angles shows little distortion between the polymethine plane and the flavylium heterocycles when the dimethylamino group is at the six-, seven-, or right- position (α = 5°–7°, Figure 3B). At the five-position, the NMe_2 C-H bonds clash with the vinyl C-H bond of the polymethine chain, which results in a larger angle of 18°.

The NMe_2 substituents also alter the geometries near the vicinity of the flavylium heterocycle. The torsion angle β in **Flav7** (**1**) and **6-Flav7** (**4**) are nearly planar (5° and 1°, respectively). **5-Flav7** (**3**) and **8-Flav7** (**5**) have β angles of 46° and 44°, respectively, which indicate significant out-of-plane distortions. The NMe_2 groups rotate to minimize closed-shell repulsion to the vinyl C-H bond in **5-Flav7** (**3**, Figure 3C) and to the oxygen lone pair and adjacent C-H bond of the phenyl group in **8-Flav7** (**5**, Figure 3D).

We computed the frontier molecular orbitals (FMOs) to illustrate the differences in the electronic structures of these fluorophores. Displayed in Figures 4A and Figure S3 are the highest occupied molecular orbitals and lowest unoccupied molecular orbitals (HOMOs and LUMOs). The FMOs show that the extent of π-conjugation in the flavylium heterocycles varies with respect to the substituent site. **Flav7** (**1**) and **6-Flav7** (**4**) have dimethylamino substituents that are nearly coplanar with flavylium heterocycles, allowing for the NMe_2 to maximally extended orbital overlap in the HOMOs and LUMOs. This results in reduced HOMO-LUMO gaps and longer $\lambda_{max,abs}$. The 46° out-of-plane torsion in **5-Flav7** (**3**) results in decreased π-conjugation of the nitrogen lone pair to the chromophore. The substantial out-of-plane distortion of **8-Flav7** (**5**) nearly eliminates π-conjugation of the nitrogen lone pair, which leads to unperturbed $\lambda_{max,abs}$ relative to parent dye, **IR-27** (**2**).

The predicted $\lambda_{max,abs}$ values of dyes were calculated using configuration interactions of singles with corrections to doubles method (CIS(D))[30,31] and the cc-pVDZ basis sets. The computed HOMO–LUMO gaps match the experimentally observed trend (Figure 4B). **6-Flav7** (**4**) has the smallest gap (2.94 eV), which correlates with the longest $\lambda_{max,abs,}$ whereas **8-Flav7** (**5**) has the largest gap (3.03 eV) and the shortest experimentally determined $\lambda_{max,abs}$. The predicted $\lambda_{max,abs}$ is systematically blue-shifted 159–190 nm relative to experimental, likely due to contributions from double excitation that are unaccounted for with single-reference quantum mechanical methods.[32,33]

Our analysis of the λ_{max} show that the position of substituents on the flavylium ring can affect $\lambda_{max,}$ comparable to the magnitude observed by varying the electronics at the seven-position. However, the major limitation of small molecule fluorophores in the SWIR is their low $\Phi_{F.}$[21] At 0.61%, **Flav7** (**1**) has a respectable Φ_F for polymethine SWIR fluorophores. It is of interest to gain an understanding of how structural modifications impact Φ_F to develop brighter probes. Previously, we found that functional groups at the seven-position showed little change in quantum yield of fluorescence.[25] However, here we see that substituent placement can greatly alters the Φ_F (Figure 2).

We measured Φ_F values for **5-Flav7**, **6-Flav7**, and **8-Flav7** (**3–5**). All three were significantly less fluorescent than **Flav7** (**1**), with Φ_F ranging from 0.12–0.16%. We were particularly interested in the large difference between **Flav7** (**1**) and **6-Flav7** (**4**), which are conformationally similar. Flavylium heterocycles are structurally similar to coumarin heterocycles, and large differences in Φ_F between six- and seven-position substituted coumarin fluorophores has previously been observed.[27] The low Φ_F in 6-aminocoumarins (**10**) compared to 7-aminocoumarins (**11**) was attributed to a significant contribution of a twisted intermolecular charge transfer (TICT) state in which the amine donor twists out of plane by ~90° upon photoexcitation, forming a non-emissive species.[34,35] We hypothesized a similar phenomenon could contribute to the loss of fluorescence in **6-Flav7** (**4**), as compared with the parent **Flav7** (**1**).

To gain insight into whether TICT was contributing to observed differences in fluorescence **1** and **4**, we synthesized a flavylium heptamethine that contained an azetidine at the six-position. Azetidines have been shown to minimize TICT states by preventing the substituent from twisting out of plane.[36] **Azet-6-Flav7** (**12**, Figure 5A) was synthesized following a similar procedure to **6-Flav7** (Scheme S1). We found the Φ_F to be 0.21%, 1.75 times higher than the dimethylamino derivative. In contrast, azetidine at the 7-position (**13**) resulted in a slight decrease in Φ_F compared with **Flav7** (**1**) (0.51% vs. 0.61%, Figure 5C).[25] We calculated fold change of in Φ_F for each of the pairs of six- and seven-substituted fluorophores (**4** vs **1**, **12** vs **13, 10** vs **11**; Figure 5D) and found that the NMe_2 variants of both flavylium heptamethine and coumarin dyes had similar changes, whereas the azetidine functionalized Flav7 dyes displayed a reduced change. These data support the notion that TICT could be playing a larger role at the six-position, contributing to the observed difference in Φ_F between **Flav7 (1)** and **6-Flav74** vs (**4**).

Conclusions

In conclusion, we have demonstrated that dimethylamino substituent placement significantly influences the photophysical properties of flavylium heptamethine dyes. Substituent steric effects impact the degree of conjugation and alter the $\lambda_{max,abs.}$ We have used density functional theory calculations to understand the origin of these unique photophysical properties. The seven-position appears to be advantageous for obtaining a high quantum yield and maintaining SWIR absorption maxima; however, further red-shifted dyes can be obtained by substituting the six-position. The insights garnered herein can contribute to the design of novel fluorophores to be utilized for high resolution SWIR *in vivo* imaging.

Supplementary Material

Refer to Web version on PubMed Central for supplementary material.

ACKNOWLEDGMENT

This work was supported by grants from the Sloan Foundation (FG-2018-10855 to E.M.S.), NIH (1R01EB027172-01 to E.M.S.), and NSF (NSF-1940307 to S.A.L.; CHE-1905242 to E.M.S.). Instrumentation was funded through the NSF MRI (CHE-1048804) and NIH (1S10OD016387-01). S.A.L, and J.L. acknowledge the Massachusetts Green High-Performance Computing Center (MGHPCC) for computing resources and the staff of Research Computing for support. We thank Dr. J. Cox (Northeastern), P. Neal (Northeastern), I. Lim (UCLA) and E. Cosco (UCLA) for helpful discussions.

REFERENCES

(1). Schnermann MJ Chemical Biology: Organic Dyes for Deep Bioimaging. Nature. 2017, 551, 176–177. [PubMed: 29088708]

(2). Thimsen E; Sadtler B; Berezin MY Shortwave-Infrared (SWIR) Emitters for Biological Imaging: A Review of Challenges and Opportunities. Nanophotonics 2017, 6 (5), 1043–1054.

(3). Weissleder R A Clearer Vision for in Vivo Imaging. Nat. Biotechnol 2001, 19 (4), 316–317. [PubMed: 11283581]

(4). Smith AM; Mancini MC; Nie S Bioimaging: Second Window for in Vivo Imaging. Nat. Nanotechnol 2009, 4, 710–711. [PubMed: 19898521]

(5). Carr JA; Franke D; Caram JR; Perkinson CF; Saif M; Askoxylakis V; Datta M; Fukumura D; Jain RK; Bawendi MG; Bruns OT Shortwave Infrared Fluorescence Imaging with the Clinically Approved Near-Infrared Dye Indocyanine Green. Proc. Natl. Acad. Sci 2018, 115 (17), 4465–4470. [PubMed: 29626132]

(6). Hong G; Lee JC; Robinson JT; Raaz U; Xie L; Huang NF; Cooke JP; Dai H Multifunctional in Vivo Vascular Imaging Using Near-Infrared II Fluorescence. Nat. Med 2012, 18 (12), 1841–1846. [PubMed: 23160236]

(7). Welsher K; Liu Z; Sherlock SP; Robinson JT; Chen Z; Daranciang D; Dai H A Route to Brightly Fluorescent Carbon Nanotubes for Near-Infrared Imaging in Mice. Nat. Nanotechnol 2009, 4 (11), 773–780. [PubMed: 19893526]

(8). Diao S; Blackburn JL; Hong G; Antaris AL; Chang J; Wu JZ; Zhang B; Cheng K; Kuo CJ; Dai H Fluorescence Imaging In Vivo at Wavelengths beyond 1500 Nm. Angew. Chemie Int. Ed 2015, 54 (49), 14758–14762.

(9). Robinson JT; Hong G; Liang Y; Zhang B; Yaghi OK; Dai H In Vivo Fluorescence Imaging in the Second Near-Infrared Window with Long Circulating Carbon Nanotubes Capable of Ultrahigh Tumor Uptake. J. Am. Chem. Soc 2012, 134 (25), 10664–10669. [PubMed: 22667448]

(10). Naczynski DJ; Tan MC; Zevon M; Wall B; Kohl J; Kulesa A; Chen S; Roth CM; Riman RE; Moghe PV Rare-Earth-Doped Biological Composites as in Vivo Shortwave Infrared Reporters. Nat. Commun 2013, 4, 2199. [PubMed: 23873342]

(11). Naczynski DJ; Tan MC; Riman RE; Moghe PV Rare Earth Nanoprobes for Functional Biomolecular Imaging and Theranostics. J. Mater. Chem. B 2014, 2, 2958–2973. [PubMed: 24921049]

(12). Naczynski DJ; Sun C; Türkcan S; Jenkins C; Koh AL; Ikeda D; Pratx G; Xing L X-Ray-Induced Shortwave Infrared Biomedical Imaging Using Rare-Earth Nanoprobes. Nano Lett. 2015, 15 (1), 96–102. [PubMed: 25485705]

(13). Bruns OT; Bischof TS; Harris DK; Franke D; Shi Y; Riedemann L; Bartelt A; Jaworski FB; Carr JA; Rowlands CJ; et al. Next-Generation in Vivo Optical Imaging with Short-Wave Infrared Quantum Dots. Nat. Biomed. Eng 2017, 1 (4).

(14). Dong B; Li C; Chen G; Zhang Y; Zhang Y; Deng M; Wang Q Facile Synthesis of Highly Photoluminescent Ag2Se Quantum Dots as a New Fluorescent Probe in the Second Near-Infrared Window for in Vivo Imaging. Chem. Mater 2013, 25 (12), 2503–2509.

(15). Hong G; Robinson JT; Zhang Y; Diao S; Antaris AL; Wang Q; Dai H In Vivo Fluorescence Imaging with Ag 2 S Quantum Dots in the Second Near-Infrared Region. Angew. Chemie Int. Ed 2012, 51 (39), 9818–9821.

(16). Yang ST; Wang X; Jia G; Gu Y; Wang T; Nie H; Ge C; Wang H; Liu Y Long-Term Accumulation and Low Toxicity of Single-Walled Carbon Nanotubes in Intravenously Exposed Mice. Toxicol. Lett 2008, 181 (3), 182–189. [PubMed: 18760340]

(17). Liu Z; Davis C; Cai W; He L; Chen X; Dai H Circulation and Long-Term Fate of Functionalized, Biocompatible Single-Walled Carbon Nanotubes in Mice Probed by Raman Spectroscopy. Proc. Natl. Acad. Sci. U. S. A 2008, 105 (5), 1410–1415. [PubMed: 18230737]

(18). Choi HS; Liu W; Misra P; Tanaka E; Zimmer JP; Bawendi MG; Frangioni JV Renal Clearance of Quantum Dots. Nat. Biotechnol/ 2007, 25 (10), 1165–1170.

(19). Fitzpatrick JAJ; Andreko SK; Ernst LA; Waggoner AS; Ballou B; Bruchez MP Long-Term Persistence and Spectral Blue Shifting of Quantum Dots in Vivo. Nano. Lett 2009, 9 (7), 2736–2741. [PubMed: 19518087]

(20). Lavis LD; Raines RT Bright Ideas for Chemical Biology. ACS Chem. Biol 2008, 3 (3), 142–155. [PubMed: 18355003]

(21). Casalboni M; De Matteis F; Prosposito P; Quatela A; Sarcinelli F Fluorescence Efficiency of Four Infrared Polymethine Dyes. Chem. Phys. Lett 2003, 373 (3–4), 372–378.

(22). Wang S; Fan Y; Li D; Sun C; Lei Z; Lu L; Wang T; Zhang F Anti-Quenching NIR-II Molecular Fluorophores for in Vivo High-Contrast Imaging and PH Sensing. Nat. Commun 2019, 10 (1), 1058. [PubMed: 30837470]

(23). Hong G; Zou Y; Antaris AL; Diao S; Wu D; Cheng K; Zhang X; Chen C; Liu B; He Y; et al. Ultrafast Fluorescence Imaging in Vivo with Conjugated Polymer Fluorophores in the Second Near-Infrared Window. Nat. Commun 2014, 5 (1), 1–9.

(24). Cosco ED; Caram JR; Bruns OT; Franke D; Day RA; Farr EP; Bawendi MG; Sletten EM Flavylium Polymethine Fluorophores for Near- and Shortwave Infrared Imaging. Angew. Chemie Int. Ed 2017, 56 (42), 13126–13129.

(25). Cosco ED; Spearman AL; Ramakrishnan S; Lingg JGP; Saccomano M; Pengshung M; Arus BA; Wong KCY; Glasl S; Ntziachristos V; Warmer M; McLaughlin RR; Bruns OT; Sletten EM

Shortwave infrared polymethine fluorophores matched to excitation lasers enable noninvasive, multicolor in vivo imaging in real time. Nat. Chem 2020, in revision.

(26). Hansch C; Leo A; Taft RW A Survey of Hammett Substituent Constants and Resonance and Field Parameters. Chem. 1991, 91, 165–195.

(27). Purification of 8-Flav7 was attempted via silica column chromatography, HPLC, recrystallization, and washing with solvents (toluene, tetrahydrofuran, diethyl ether, ethyl acetate). No Title.

(28). Zhao Y; Truhlar DG The M06 Suite of Density Functionals for Main Group Thermochemistry, Thermochemical Kinetics, Noncovalent Interactions, Excited States, and Transition Elements: Two New Functionals and Systematic Testing of Four M06-Class Functionals and 12 Other Functionals. Theor. Chem. Acc 2008, 120 (1–3), 215–241.

(29). Scalmani G; Frisch MJ Continuous Surface Charge Polarizable Continuum Models of Solvation. I. General Formalism. J. Chem. Phys 2010, 132 (11), 114110. [PubMed: 20331284]

(30). Head-Gordon M; Rico RJ; Oumi M; Lee TJ A Doubles Correction to Electronic Excited States from Configuration Interaction in the Space of Single Substitutions. Chem. Phys. Lett 1994, 219 (1–2), 21–29.

(31). Head-Gordon M; Maurice D; Oumi M A Perturbative Correction to Restricted Open Shell Configuration Interaction with Single Substitutions for Excited States of Radicals. Chem. Phys. Lett 1995, 246 (1–2), 114–121.

(32). Zhou P Why the Lowest Electronic Excitations of Rhodamines Are Overestimated by Time-Dependent Density Functional Theory. Int. J. Quantum Chem 2018, 118 (23), e25780.

(33). CIS(D) leads to smaller deviations relative to TD-DFT methods because of the built-in corrections to the doubly excited state. No Title.

(34). Rettig W; Klock A Intramolecular Fluorescence Quenching in Aminocoumarines. Identification of an Excited State with Full Charge Separation. Can. J. Chem 1985, 63, 1649.

(35). An azetidine substituted at the seven-position of coumarin has been previously synthesized and has shown some TICT character in water. Grimm JB; English BP; Chen J; Slaughter JP; Zhang Z; Revyakin A; Patel R; Macklin JJ; Normanno D; Singer RH; et al. A General Method to Improve Fluorophores for Live-Cell and Single-Molecule Microscopy. Nat. Methods 2015, 12 (3), 244–250. [PubMed: 25599551]

(36). Liu X; Qiao Q; Tian W; Liu W; Chen J; Lang MJ; Xu Z Aziridinyl Fluorophores Demonstrate Bright Fluorescence and Superior Photostability by Effectively Inhibiting Twisted Intramolecular Charge Transfer. J. Am. Chem. Soc 2016, 138, 6963.

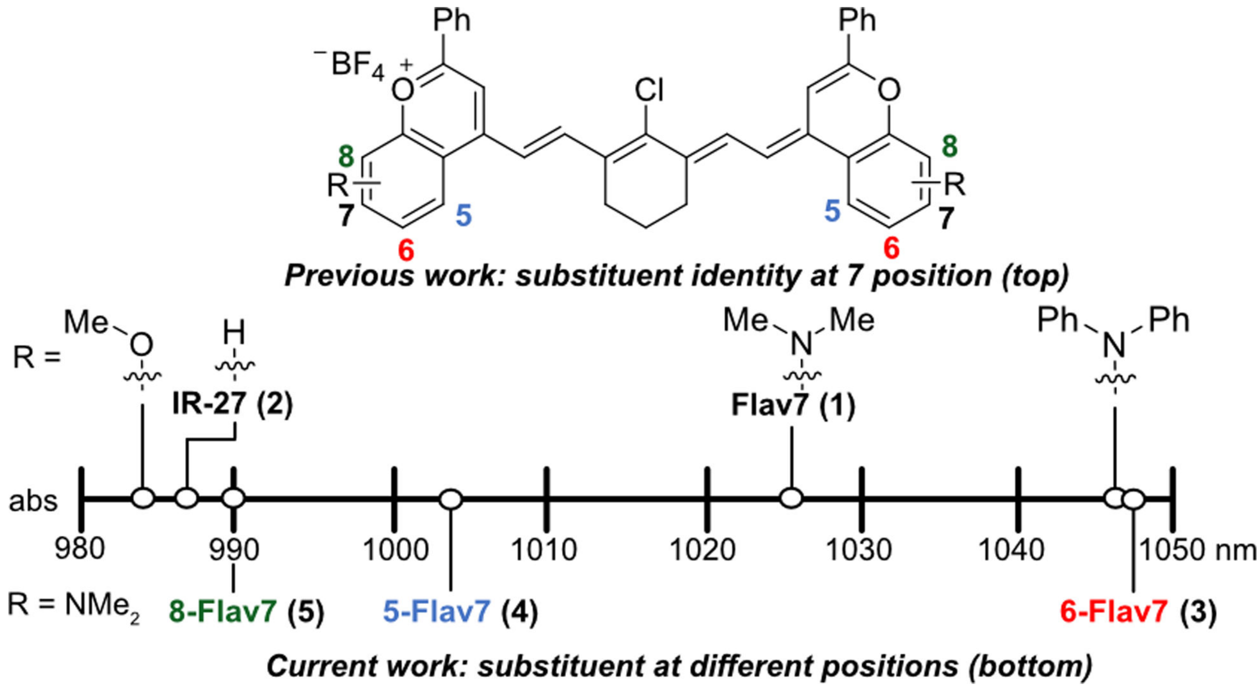

Figure 1.

Systematic exploration of structural modifications of Flav7 (**1**). Previous work on derivatives at the seven-position, includeing methoxy and diphenylamine with a shift in λ_{max}.[25] Current work on exploring dimethylamino substitutions at different positions (five-, six-, and eight- on the heterocycle (**3–5**).

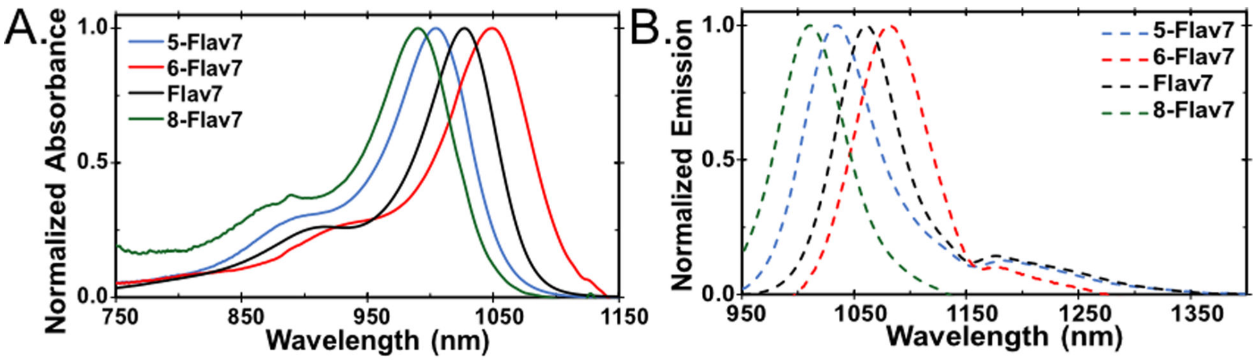

C.

Compound	$\lambda_{max, abs}$ (nm)	$\lambda_{max,em}$(nm)	Φ_F (%)	ε (x 10^5 M^{-1} cm^{-1})
IR-27 (2)[a]	987	1011	0.35 ± 0.01	2.31 ± 0.06
5-Flav7 (3)	1004	1036	0.14 ± 0.01	0.13 ± 0.07
6-Flav7 (4)	1048	1080	0.12 ± 0.01	1.6 ± 0.3
Flav7 (1)[a]	1027	1053	0.61 ± 0.02	2.41 ± 0.01
8-Flav7 (5)[b]	990	1015	0.16 ± 0.01	N/A

Figure 2.
Normalized (A) absorbance and (B) emission of the flavylium polymethines discussed. (C) Photophysical data of unsubstituted (**IR-27**, **2**) and dimethylamino substituted heptamethines (**1**, **3–5**). All samples were taken in dichloromethane. [a]Data was previously reported.[25] [b]Photophysical data was taken with crude sample.

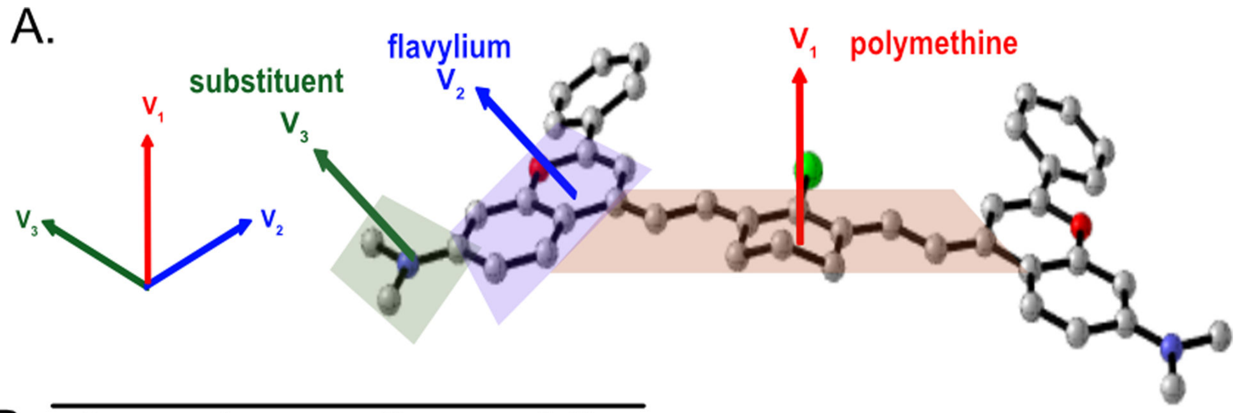

B.

Compound	α (°)	β (°)
IR-27	7	N/A
5-Flav7	18	46
6-Flav7	7	5
Flav7	5	1
8-Flav7	6	44

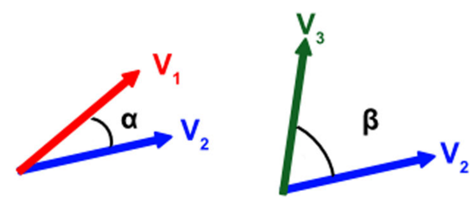

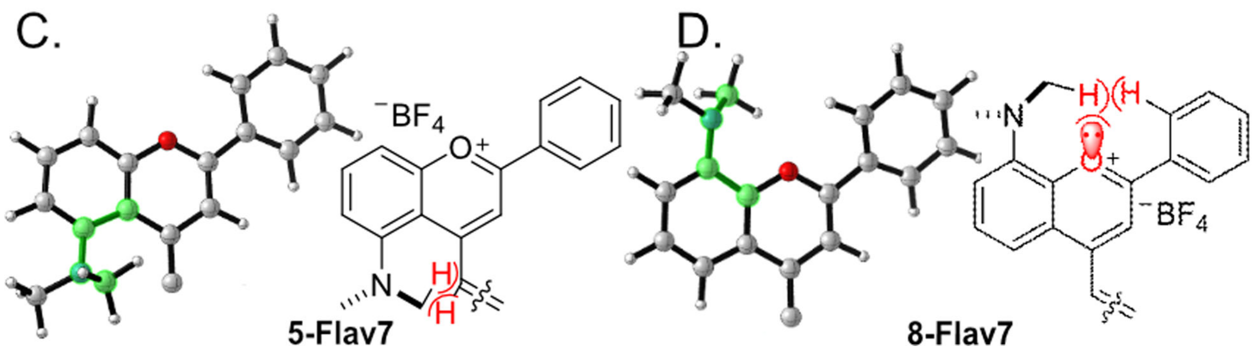

Figure 3.

(A) Represented by **Flav7**; torsion angles are defined by α (V_1 to V_2, red to blue) and β (V_3 to V_2, green to blue) using the normal of the plane of the polymethine (V_1), flavylium (V_2) and substituent (V_3). (B) Table of α and β angles for **Flav7** dyes. (C,D) Heterocycle structures of (C) **5-Flav7** and (D) **8-Flav7** at the S_0 state, optimized with M06–2X/6–31+G(d,p). The polymethine chain is omitted for clarity. The dihedral angles at the substituted positions of the flavylium heterocycles are highlighted in green to show the rotation of the NMe_2 group in **5-Flav7** and **8-Flav7**.

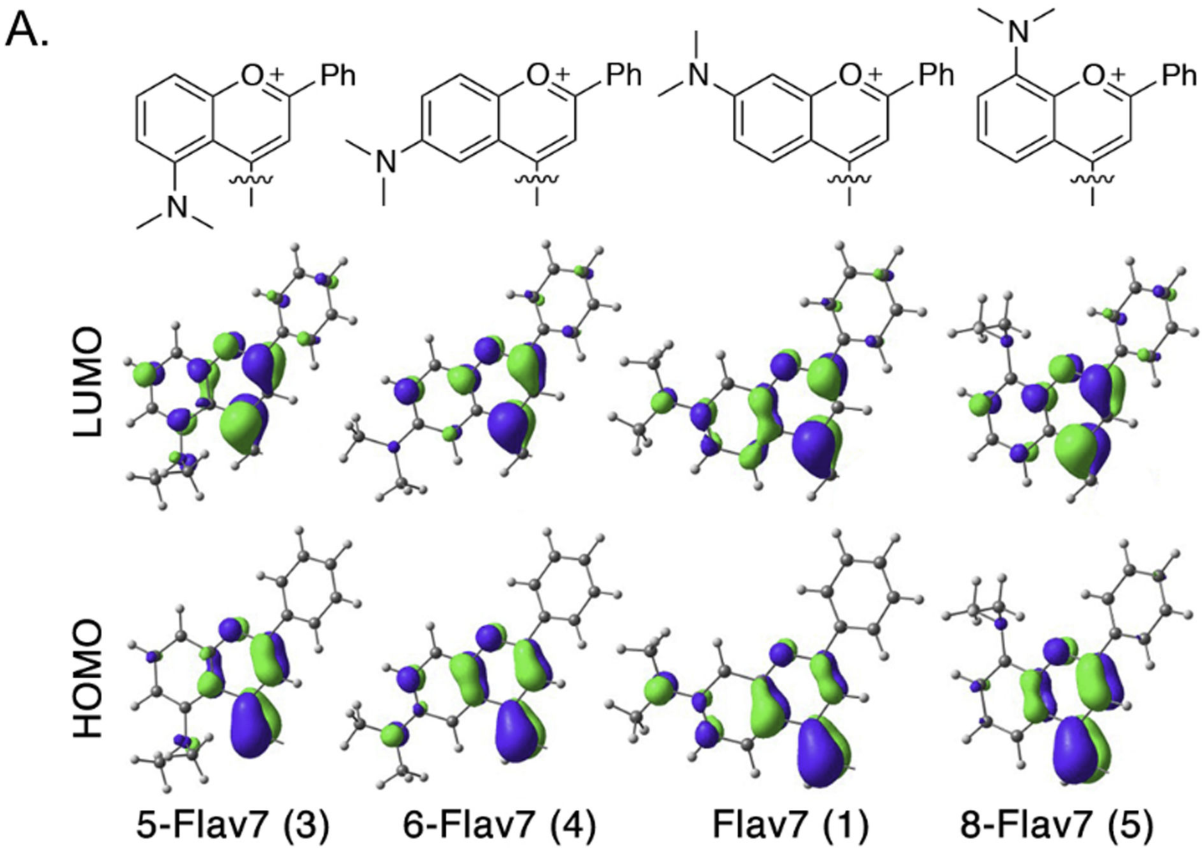

B.

Compound	$\lambda_{max, calc. abs}$ (nm)	Δ (nm)	HOMO-LUMO gap (eV)
IR-27 (2)	822	165	3.03
5-Flav7 (3)	835	169	2.99
6-Flav7 (4)	858	190	2.94
Flav7 (1)	864	163	2.98
8-Flav7 (5)	831	159	3.03

Figure 4.

(A) HOMOs and LUMOs of **Flav7** (**1**) and (**5**,**6** and **8**)**-Flav7** (**3–5**) at M06–2X/6–31+G(d,p) level of theory. Polymethine chains were omitted for clarity. Explicit frontier molecular orbital information can be found in the SI. (B) Table of calculated $\lambda_{max,calc,abs}$ (nm) determined by theoretical HOMO-LUMO gap (eV). Δ is the difference between experimental and calculated $\lambda_{max,abs}$.

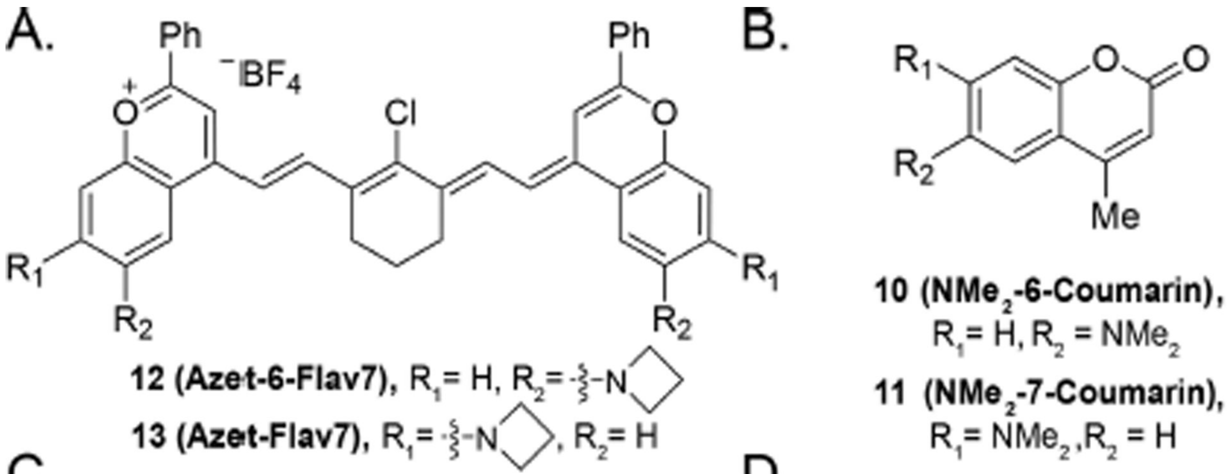

C.

Compound	Φ_F (%)
Flav7 (1)[a]	0.61 ± 0.01
Azet-Flav7 (13)[a]	0.51 ± 0.01
6-Flav7 (4)	0.12 ± 0.01
Azet-6-Flav7 (12)	0.21 ± 0.01
NMe$_2$-6-Coumarin (10)[b]	0.20
NMe$_2$-7-Coumarin (11)[b]	0.80

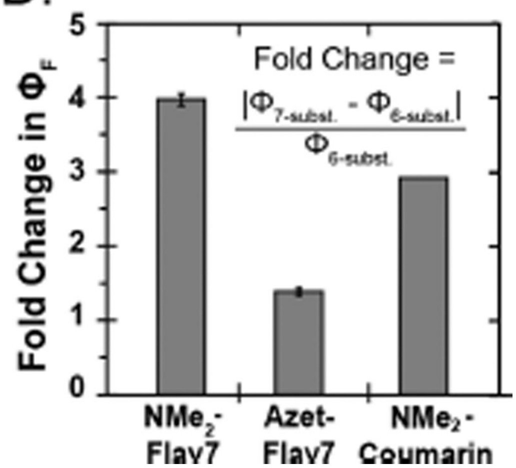

Figure 5.

(A) Structures of azetidine-substituted flavylium heptamethines (**12, 13**). (B) Structure of 6- and 7-aminocoumarins (**10, 11**). (C) Φ_F of flavylium heptamethine and coumarin dyes in dichloromethane and decanol, respectively. [a]Previously reported by our group.[25] [b]Previously reported.[34] (D) Fold change of Φ_F between six- and seven-substituted flavylium heptamethine or coumarin fluorophore.

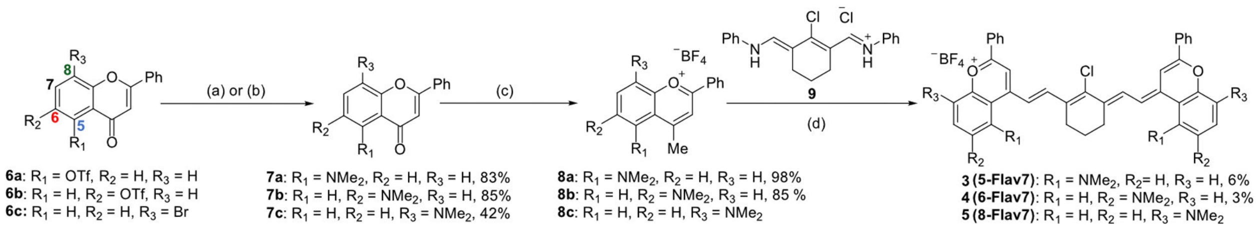

Scheme 1.

Synthetic scheme for dimethylamino flavylium heptamethines **3–5** with substituents at the five-, six-, and eight- positions. (a) RuPhos Pd G3 (0.10 eq), RuPhos (0.10 eq), Cs_2Co_3, $HNMe_2$, toluene, 110 °C, 24 h. for **6a** and **6b**. (b) SPhos Pd G3 (0.10 eq), SPhos (0.10 eq) Cs_2Co_3, $HNMe_2$, toluene, 110 °C, 24 h. for **6c**. (c) MeMgBr (1.4M), THF, r.t. d) 2,6-di-*tert*-butyl-4methyl-pyridine, *n*-butanol/toluene or acetic anhydride, 100 °C, 15 min. Refer to SI for further experimental details.